Reduction of Drag Penalty by means of Plain Flaps in the Boomless Busemann Biplane

Hiroshi Yamashita* **and Shigeru Obayashi†**
Tohoku University, 2-1-1 Katahira, Aoba-ku, Sendai-shi, Miyagi, 980-8577, Japan
Email: yamashita@edge.ifs.tohoku.ac.jp; obayashi@ifs.tohoku.ac.jp

Kazuhiro Kusunose‡
Formerly Institute of Fluid Science, Tohoku University and Currently Technical Research and Development Institute, Ministry of Defense, 1-2-10 Sakae-cho, Tachikawa-shi, Tokyo, 190-8533, Japan
Email: kusunose@cs.trdi.mod.go.jp

Abstract
This study describes a method to overcome the choked-flow and flow-hysteresis problems of the Busemann biplane at off-design conditions, by using plain flaps at the leading and trailing edges. Two-dimensional analyses of four different biplanes were addressed in order to examine the effect of the flaps, using Computational Fluid Dynamics (CFD) in inviscid flow (Euler) mode. Results show that the leading-edge flaps can alleviate the drag increase due to the choked-flow, and reduce the area of flow-hysteresis. In contrast, the trailing-edge flaps are not effective in overcoming these problems. However, the trailing-edge flaps can reduce the wave drag near to the speed of sound, and also shift the drag-divergence Mach number to a higher one. Thus, the combined effect of both flaps allows us to smoothly achieve the design point ($M_\infty = 1.7$) from subsonic regime, and to avoid the severe drag penalty due to the choked-flow and flow-hysteresis problems.

NOMENCLATURE

A_i	=	inlet area
A_t	=	throat area
c	=	chord
C_d	=	wave drag coefficient
C_p	=	pressure coefficient
M_∞	=	free-stream Mach number
t	=	airfoil thickness
α	=	angle of attack
β	=	shock-wave angle
γ	=	ratio of specific heats
ε	=	wedge angle of the Busemann biplane

1. INTRODUCTION

In 2003, the first successful supersonic transport (SST), the Concorde[1] (1969 – 2003), ceased its operations and flight services. This means that, without a complete development of the next-generation SST,[2,3] commercial airplanes today can only fly at transonic speeds. It is important to note, however, that the Concorde had already flown for over 30 years, although our aviation history comprises only about 100 years. These 30 years of flight are a truly admirable achievement and have given us great knowledge, technologies and significant challenges.

*Graduate student, Institute of Fluid Science.

†Professor, Institute of Fluid Science.

‡Senior Research Scientist, Technical Research and Development Institute, Ministry of Defense.

As for the development of the next supersonic aircraft, there is an important problem that needs to be overcome; the sonic boom problem.[4-7] Sonic boom is a phenomenon caused by the shock waves propagating from an airplane at supersonic speed, which leads to a very loud sound resembling a thunder on the ground. Therefore, commercial airplanes are prohibited to fly over land at supersonic speed due to the loudness of sonic boom.[8]

For this issue, considerable research has been conducted to test different sonic boom reduction technologies. In 2003, for example, the F-5 Shaped Sonic Boom Demonstration (SSBD) program was performed to assess the shaped boom signature.[9-12] Also, from 2006 to 2007, the Quiet Spike Flight Test program was conducted by Gulfstream Aerospace Corporation in order to demonstrate the feasibility of the extendable nose spike (i.e., the Quiet Spike) used for sonic boom suppression.[13-17] Both programs successfully demonstrated their concept of sonic boom reduction and showed the potential of their approaches. Even now, several projects are involved with the design of low boom configurations.[18]

In our research, we have addressed the biplane concept proposed by Kusunose[19,20] which enables a significant reduction, if not complete elimination, of shock waves. Fundamentally, for two-dimensional airfoils, wave drag may be separated into drag due to lift (including the camber effect of the airfoils) and drag due to thickness in supersonic flow.[21] In spite of the fact that wave drag due to lift cannot be eliminated completely; it can be reduced significantly by using multi-airfoil configurations. These configurations re-distribute the system's total lift among the individual airfoil elements, reducing the lift of each individual element and the total wave drag of the system. We call this the "wave reduction

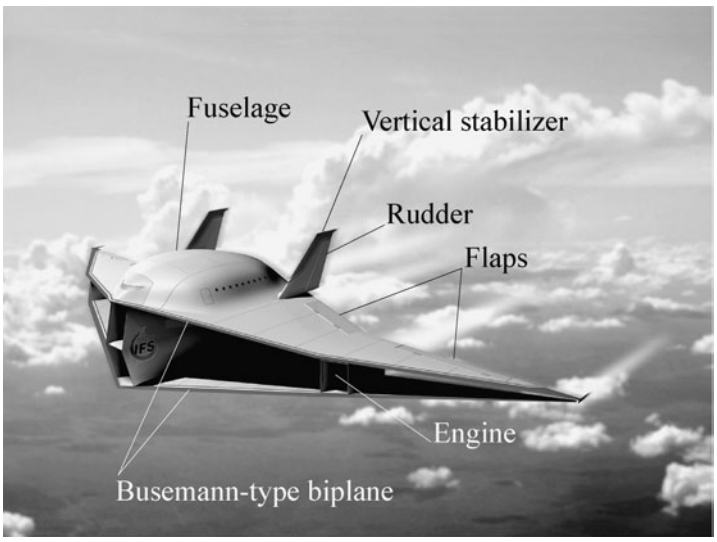

a) Supersonic level flight

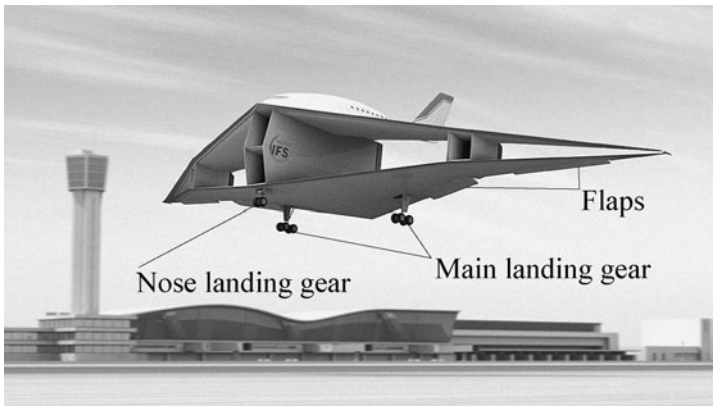

b) Takeoff and landing

Figure 1. Conceptual drawing of a boomless supersonic biplane. Cruise Mach number is assumed as M_∞ = 1.7 for supersonic level flight.

effect." In the same way, the wave drag due to thickness can also be almost eliminated by using a biplane configuration, which depends on mutual cancellation of waves between the two airfoil elements. This will be referred to as the "wave cancellation effect" hereinafter in this paper. For these reasons, an ideal boomless biplane configuration can be designed by applying these two effects.[22-24] At present, Kusunose and the author's group have addressed the design of a supersonic biplane.[25-28] Figure 1 shows the conceptual drawing of boomless supersonic biplane; the cross-sectional shape of the wing is a Busemann-type biplane, and the engines are mounted between the wings.

It is, however, difficult to design an ideal boomless biplane that can fly effectively from subsonic to supersonic speed in real flight. The reason for this is that the desired wave cancellation effect, which is based on the Busemann biplane, can only be achieved at the designed Mach number and at a specific flow condition. Unfortunately, under off-design conditions, we have the phenomena of choked-flow and flow-hysteresis, which result in a severe drag penalty.[28] Therefore, it is important to formulate how a biplane airfoil, based on the Busemann biplane, will be able to overcome the choked-flow and flow-hysteresis problems under off-design conditions.

In this paper, we present a practical solution to these problems with the application of plain flaps, which may be used primarily for takeoff and landing condition, as in a high-lift device. Particularly, we investigate the four different biplanes in order to examine the effects of the leading and trailing edge flaps: The flaps are hinged to the leading and trailing edges of the Busemann biplane, and then they can change the area of the front and rear streamlines.

The paper is organized as follows: Section 2 explains the major issues to be addressed, i.e., the choked-flow and flow-hysteresis problems of the Busemann biplane at off-design conditions. Section 3 brings a brief description of the numerical models and methods for the CFD calculations. Section 4 presents the results and discussion for the four different biplanes. Finally, Section 5 concludes the present study.

2. MAJOR ISSUES

2.1 Off-design performance of the Busemann biplane

Figure 2 shows the configurations of both the baseline diamond airfoil and the Busemann biplane. The thickness-chord ratio of the diamond airfoil and Busemann biplane are t/c = 0.1 and t/c = 0.05, respectively, since it is necessary for these two airfoils to have the same total thickness to simulate an equivalent (total) airfoil thickness. The wedge angle of the diamond airfoil is therefore 11.4 deg., and the wedge angles of Busemann biplane are 5.7 deg., which is just half the angle of the diamond airfoil (as shown in Figure 2, where ε is the wedge angle of Busemann biplane). The distance between the two biplane elements is 0.5 (when the chord length is 1.0), for a theoretical minimum drag at design Mach number of 1.7.

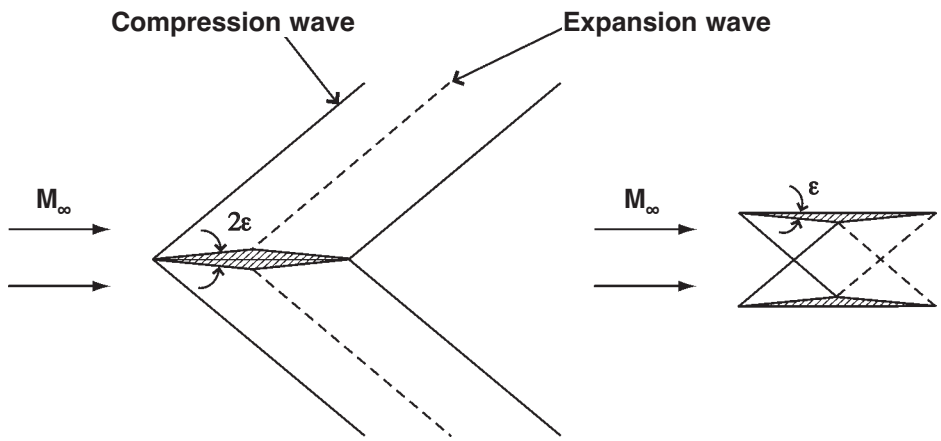

Figure 2. Configurations of both the baseline diamond airfoil (t/c = 0.1) and the Busemann biplane (t/c = 0.05). The wedge angles of the diamond airfoil and the Busemann biplane are 2ε = 11.4 degree and ε = 5.7 degree, respectively.[28]

Also, the drag characteristics of the two airfoils over a range of Mach numbers ($0.3 \le M_\infty \le 3.3$) are shown in Figure 3, using the CFD analyses in inviscid flow (Euler) mode with zero-lift conditions ($\alpha = 0$ deg.). From the results, we can confirm that the Busemann biplane, for a wide range of Mach numbers ($1.64 \le M_\infty \le 2.7$), has a wave drag lower than that of the diamond airfoil. In this low-drag range, the wave cancellation effect is critical and we hope to use this range in real flight. In decelerating condition, however, a high wave drag occurs when Mach number is $M_\infty = 1.63$ because of the appearance of a strong bow shock in front of the biplane, as shown by curve B in Figure 3. This is a choked-flow phenomenon of Busemann biplane. The C_p distributions of the Busemann biplane (including the choked-flow at $1.5 \le M_\infty \le 1.7$) are illustrated in detail in Figure 4. As the Mach number is reduced from its design Mach number ($M_\infty = 1.7$), shock waves generated by the wing elements interact with one another and a subsonic area is formed near the throat of the biplane. Eventually, the flow is choked at the maximum thickness sections between the two elements, and the subsonic area propagates upstream, forming a bow shock (as shown in Figure 4 (e)). In accelerating conditions (as shown in Figure 5), the Busemann biplane has a flow-hysteresis for a range of Mach numbers ($1.63 \le M_\infty < 2.18$). For this reason, the C_d values of the accelerating and decelerating conditions are not the same. Thus, if we would like to make the Busemann biplane reach the design point ($M_\infty = 1.7$) from subsonic regime, it needs first to exceed the Mach number $M_\infty = 2.18$, where the bow shock is swallowed backward between the wing elements.

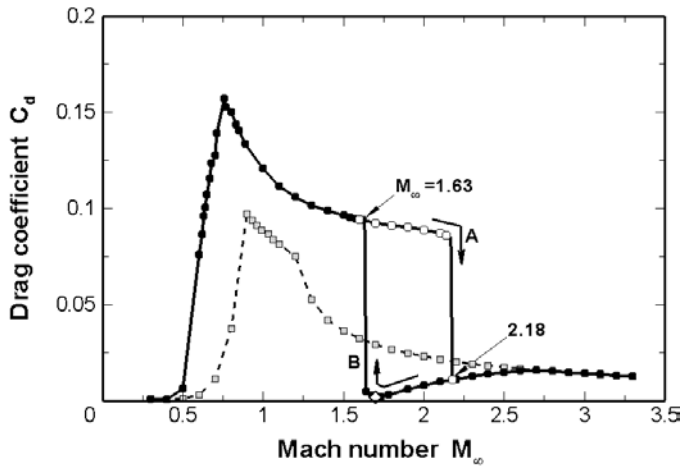

Figure 3. Comparison of the drag characteristics:[28] The solid line represents the Busemann biplane. In this case, when accelerating, C_d follows curve A. When decelerating, C_d follows curve B. The dashed line shows the baseline diamond airfoil. Also, the diamond symbol is the design point at Mach number $M_\infty = 1.7$.

2.2 Physics considerations

Before we examine how these problems can be overcome, it may be useful to discuss the start/un-start characteristics of a supersonic inlet diffuser[29] (as shown in Figure 6), because these phenomena can also be verified in the Busemann biplane. In Figure 6, the solid line shows the Kantrowitz limit.[30] Once the bow shock is generated in front of the inlets, it becomes necessary to exceed the Mach number set by the Kantrowitz limit for the inlets to go from unstart to start condition. The limit is given by eqn (1):

$$\frac{A_t}{A_i} = \left[\frac{(\gamma-1)M_\infty^2+2}{(\gamma+1)M_\infty^2}\right]^{\frac{1}{2}}\left[\frac{2\gamma M_\infty^2-(\gamma-1)}{(\gamma+1)M_\infty^2}\right]^{\frac{1}{(\gamma-1)}} \tag{1}$$

where A_i is the inlet area and A_t is the throat area. Also, the dashed line refers to the isentropic contraction limit,[29] where the Mach number is $M_\infty = 1.0$ at the throat of supersonic inlets. The isentropic contraction limit is calculated by eqn (2):

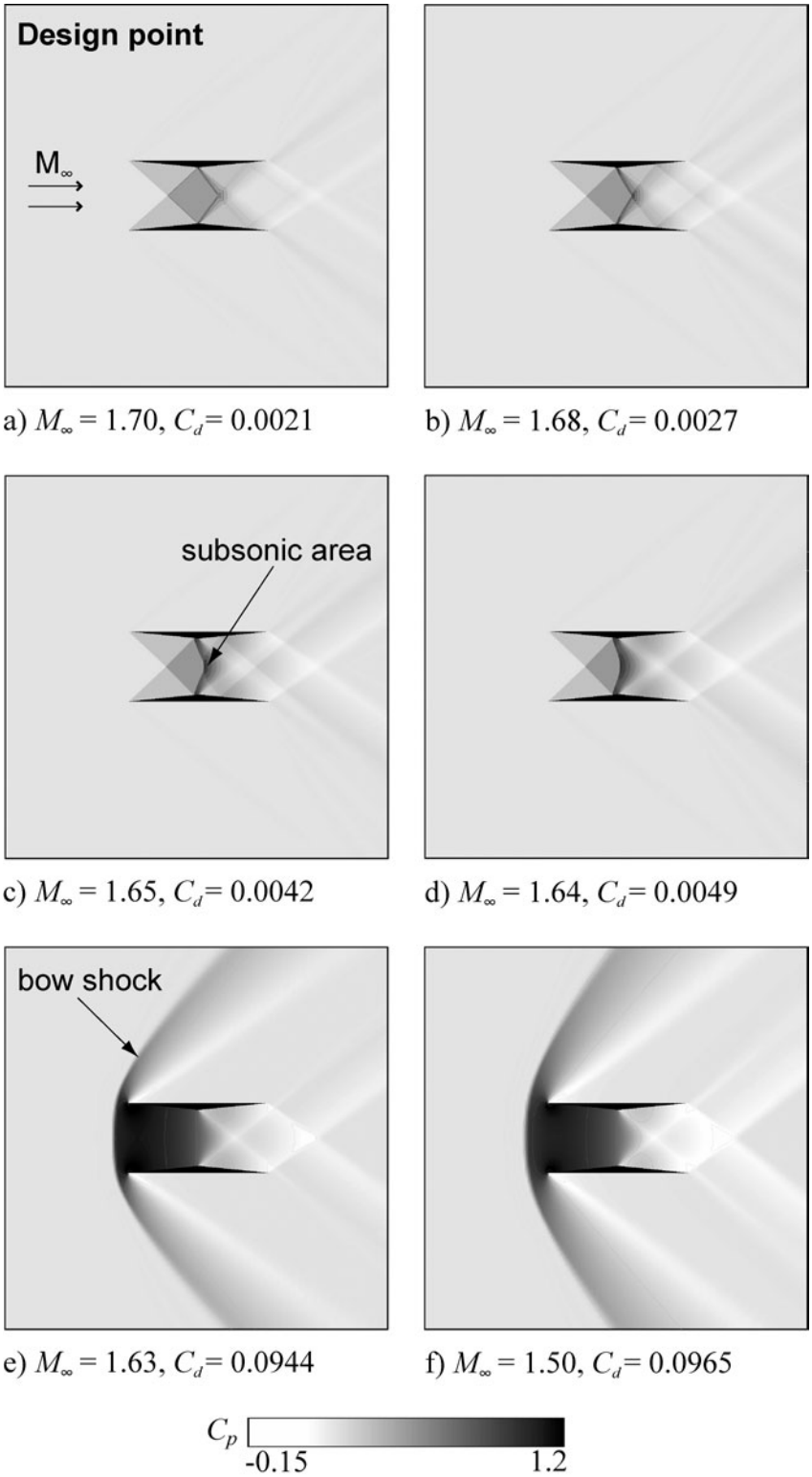

Figure 4. C_p-maps of the Busemann biplane with zero-lift in decelerating condition ($1.5 \leq M_\infty \leq 1.7$).[28]

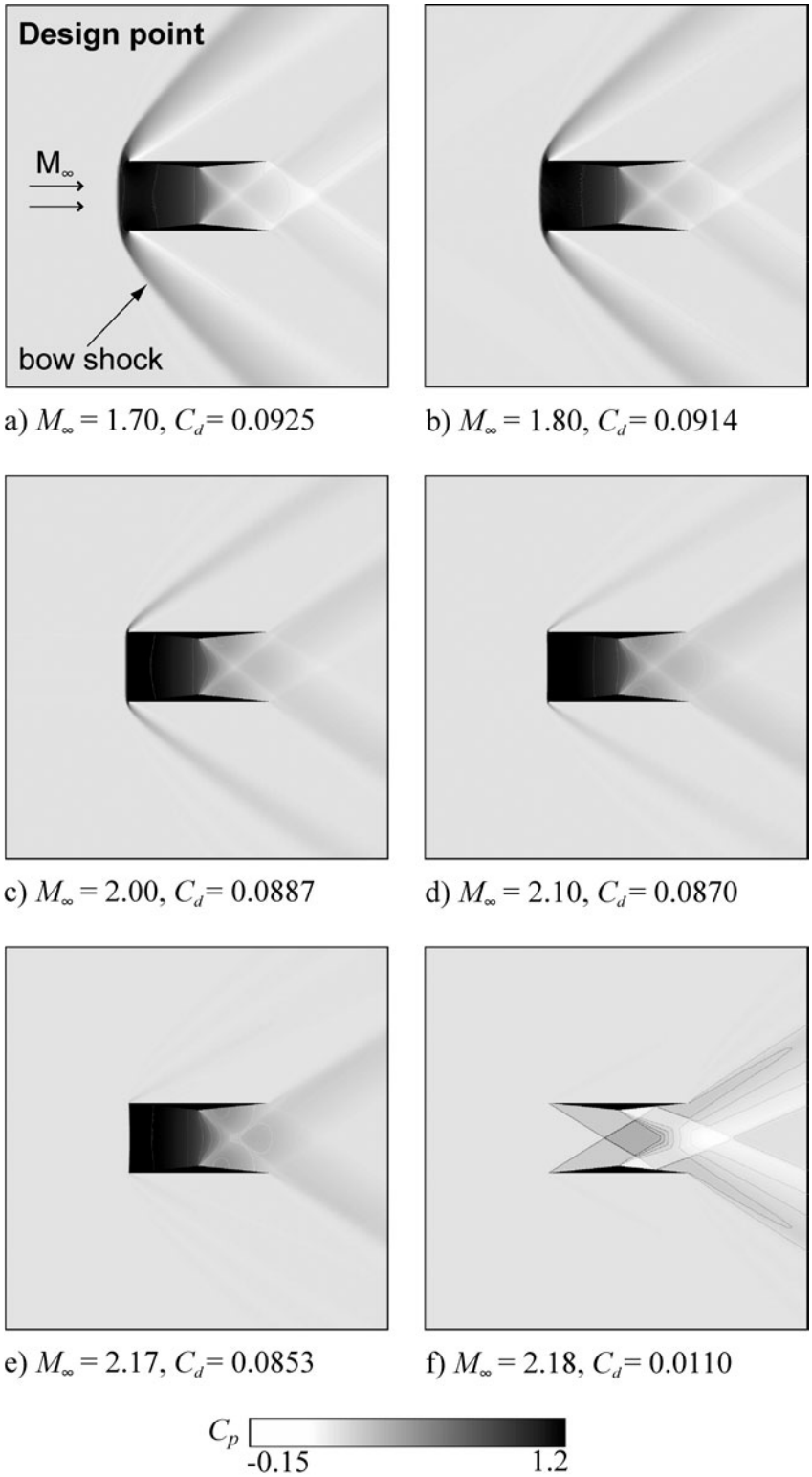

Figure 5. C_p-maps of the Busemann biplane with zero-lift in accelerating condition ($1.7 \leq M_\infty \leq 2.18$).[28]

$$\frac{A_t}{A_i} = M_\infty \left[\frac{(\gamma - 1) M_\infty^2 + 2}{\gamma + 1} \right]^{\frac{-(\gamma+1)}{2(\gamma-1)}} \tag{2}$$

It is reasonable to suppose that this rule is applicable to avoid the choked-flow and flow-hysteresis of the Busemann biplane, i.e., that the cross-section area variation of the front streamline can be helpful in overcoming these problems. In fact, the results from CFD analyses are in good agreement with the values which are calculated using eqns (1) and (2), as shown in Figures 3 and 6 (here the A_t/A_i of Busemann biplane is 0.8, as plotted by the dotted line in Figure 6). Therefore, we make an attempt to avoid the choked-flow and flow-hysteresis problems by utilizing this rule with the plain flaps in the Busemann biplane.

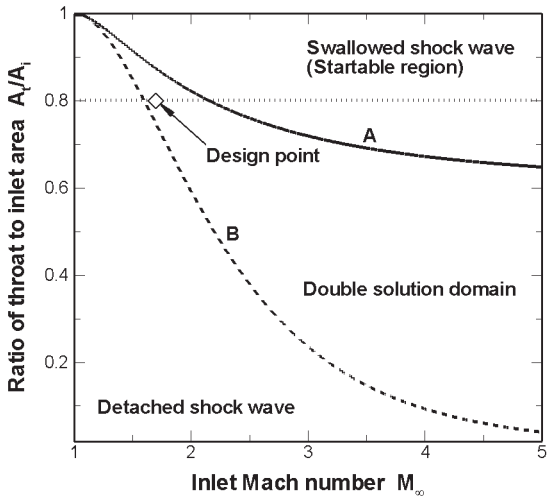

Figure 6. Start/Un-start characteristics of a supersonic inlet diffuser: The solid line (curve A) shows the Kantrowitz limit; the dashed line (curve B) shows the isentropic contraction limit. Here, the ratio of throat-to-inlet-area of the Busemann biplane is A_t/A_i = 0.8, as shown by the dotted line. The diamond symbol represents the design point of the Busemann biplane at Mach number 1.7.

3. NUMERICAL MODELS AND METHODS

In this study, the four different biplanes were investigated, as shown in Figure 7. The Euler equation is solved for all configurations by the CFD tool (UPACS-code[31]), developed at the Japan Aerospace Exploration Agency (JAXA). Actually, if we examine the detailed mechanisms of the choked-flow and flow-hysteresis phenomena, then it becomes important to use the Navier-Stokes equation for the CFD analysis. In our research, however, we simply focus on whether these phenomena occur under off-design conditions or not. Therefore, the Euler code for CFD analysis is appropriate for the objectives of the present study. The following sections describe the configurations of the four biplanes and the calculation methodology in detail.

Here, it is important to note the accuracy of the CFD analysis by using the UPACS-code. Table 1 shows the comparison between the CFD and the analytical results at Mach number M_∞ = 1.7 for several configurations, such as a single flat plate airfoil, parallel flat plate airfoils, a diamond airfoil, and the Busemann biplane. In the analyses, the single flat plate airfoil and the parallel flat plate airfoils were simulated in Euler mode with lift conditions. On the other hand, the diamond airfoil and the Busemann biplane were calculated in Euler mode with zero-lift condition. From Table 1, we can confirm that the CFD and the analytical results derived from the supersonic thin airfoil theory[21] are, generally, in good agreement for these configurations. In addition, the results of CFD analyses show that the Busemann biplane can not completely eliminate the wave drag coefficient due to the non-linear effect which occurs in the actual wave interaction. References 20 and 25 have demonstrated these validations in more detail. Therefore, we do not further discuss these validations in this paper. Also, the detailed descriptions of the UPACS-code can be found in Ref. 31.

Table. 1 Comparison between the CFD results and the analytical results of aerodynamic performance for the four configurations.[20,25]

	CFD results		Analytical results	
	C_l	C_d	C_l	C_d
Single flat plate airfoil	0.3066	0.0322	0.3047	0.0319
Parallel flat plate airfoils	0.3045	0.0160	0.3047	0.0160
Diamond airfoil	0.0000	0.0292	0.0000	0.0291
Busemann biplane	0.0000	0.0021	0.0000	0.0000

3.1 Definition of the four biplanes

Figure 7 (a) shows the configuration of the diamond airfoil separated into two elements along the chord of the baseline diamond airfoil. We used this biplane to start our investigation regarding the avoidance of choked-flow and flow-hysteresis. The thickness-chord ratio (t/c) of the individual elements was 0.05 (because the ratio of the baseline diamond airfoil is 0.1), and the distance between the two elements was set to 0.5 (relative to the chord length of 1.0), respectively.

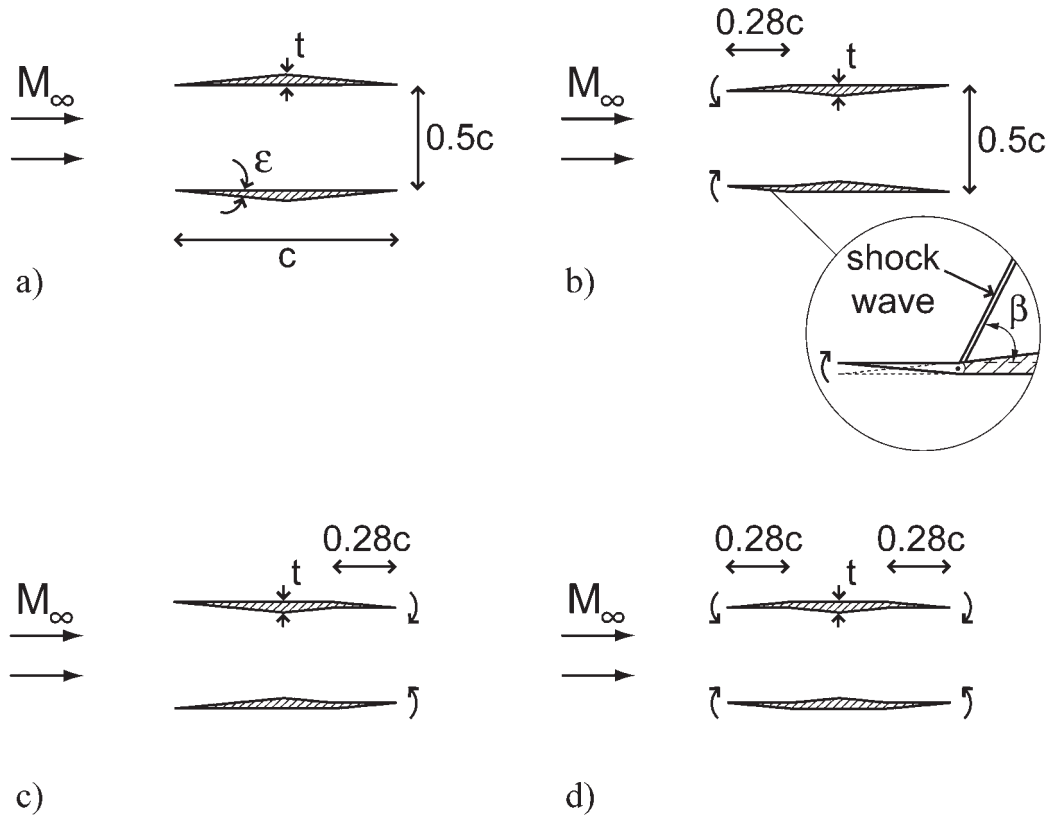

Figure 7. Comparison of biplane configurations utilized in this research: a) Diamond airfoil separated into two elements; b) Busemann biplane with deflected leading-edge flaps; c) Busemann biplane with deflected trailing-edge flaps; d) HLD-1.

In order to examine the effect of changing the area of the front streamline on choked-flow and flow-hysteresis, the Busemann biplane with deflected leading-edge flaps (as sketched in Figure 7 (b)) was investigated. This biplane is actually a Busemann biplane with its elements deflected inward from the leading-edges up to 28 % of the chord length, so as to have a configuration which is similar to plain flaps used at takeoff and landing conditions. The inner sides of the deflected parts are parallel to each other, and the uniform flow is undisturbed between them. In supersonic flow, therefore, the oblique shock waves are generated among the two elements at 28 % of the chord length, and they meet the

vertex of the triangle at the opposite elements, respectively, at $M_\infty = 1.3$ (the shock-wave angle is about $\beta = 63$ deg. at $M_\infty = 1.3$).

In the same way, the Busemann biplane with deflected trailing-edge flaps was calculated to examine the effect of changing the area of the rear streamline on choked-flow and flow-hysteresis. In this case, the Busemann biplane elements ($t/c = 0.05$) are deflected inward from the trailing-edge and back 28% of the chord length, as sketched in Figure 7 (c). Then, the inner sides of the deflected parts become parallel to each other.

Finally, we have also designed an airfoil as sketched in Figure 7 (d), which consists of a Busemann biplane with flaps at both the leading and trailing edges. This airfoil will be referred to as HLD-1 (High-Lift Device-1) in this paper, and will be utilized to investigate the combined effects of flaps in the Busemann biplane.

3.2 CFD calculation of the biplanes

The Multiblock method was applied to grid generation in all cases. Table 2 represents the number of grid points for all biplanes. As an example, Figure 8 shows the structured grid of the HLD-1 used for the 2-D analyses. Approximately 0.59 million grid points were used in total. The grid numbers around each biplane element and between these two elements were 1000 and 501×251, respectively.

The flow field for the biplane was calculated by considering flow-hysteresis. Mach numbers ranged from 0.3 to 3.3, including its design Mach number $M_\infty = 1.7$, since an airplane has to fly through subsonic, transonic, and supersonic regimes in real flight. Also, the angle of attack was set to zero for all configurations, i.e., zero-lift conditions. For the calculation of the drag coefficient, we applied the same reference chord for all biplanes as 1.0 (i.e., equal to the chord length of the baseline diamond airfoil). Additionally, in subsonic flow conditions, the C_d values of the Busemann biplane with deflected leading and trailing edges were calculated by the time averaging method, since these two biplanes, as shown in Figures 7 (b) and (c), produced an oscillatory convergence in the present calculations.

Table. 2 Number of grid points for the four biplanes.

	Total (x-y plane)	**Around each biplane element**	**Between two elements**
Diamond airfoil separated into two elements	0.42×10^6	750	251×251
Busemann biplane with deflected leading-edge flaps	0.59×10^6	1000	501×251
Busemann biplane with deflected trailing-edge flap	0.59×10^6	1000	501×251
HLD-1	0.59×10^6	1000	501×251

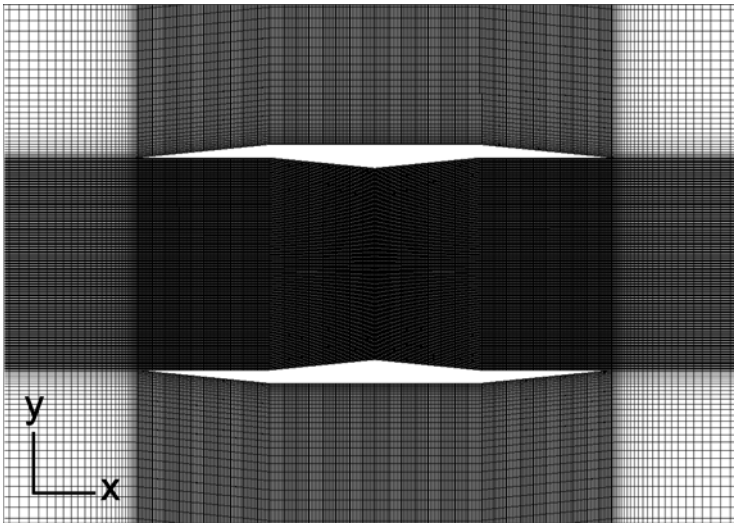

Figure 8. Structured grid of the HLD-1 used for CFD (UPACS-code) analyses.

4. RESULTS AND DISCUSSION

4.1 Diamond airfoil separated into two elements

The drag characteristics of the diamond airfoil separated into two elements are plotted in Figure 9, which also includes the drag characteristics of the Busemann biplane and the baseline diamond airfoil (given in Figure 3). It becomes clear from Figure 9 that the wave drag of the diamond airfoil separated into two elements agrees very well with that of the baseline diamond airfoil at all Mach numbers. That is, the choked-flow and flow-hysteresis do not exist for any Mach number. Also, in the light of the start/un-start characteristics of a supersonic inlet diffuser as shown in Figure 6, these results are credible since the ratio of throat-to-inlet-area of the present biplane is A_t/A_i = 1.0, i.e., the flow conditions are always within a startable region in supersonic flow. For reference purposes, the pressure coefficient contours of the present biplane and of the baseline diamond airfoil are given in Appendix A and Appendix B, respectively, for different values of free-stream Mach number.

In addition, Figure 10 shows the comparison between the pressure coefficient contours of the diamond airfoil separated into two elements and of the Busemann biplane at Mach number M_∞ = 1.5. From Figure 10, we can confirm that there is no choked-flow phenomenon with the present biplane, in contrast to the Busemann biplane for which a bow shock is generated in the upstream. Therefore, these facts suggest that it is possible to avoid the phenomena of choked-flow and flow-hysteresis in the Busemann biplane by bringing its shape close to that of the diamond airfoil separated into two elements.

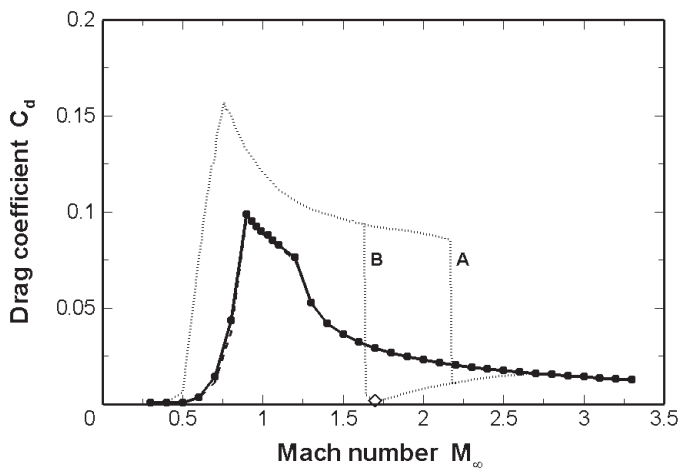

Figure 9. Comparison of drag characteristics: The solid line represents the diamond airfoil separated into two elements; the dotted line shows the Busemann biplane. In the case of the Busemann biplane, when accelerating, C_d follows curve A. When decelerating, C_d follows curve B. Also, the dashed line shows the baseline diamond airfoil. The diamond symbol is the design point at Mach number M_∞ = 1.7.

4.2 Busemann biplane with deflected leading-edge flaps

Figure 11 shows a comparison of drag characteristics for the Busemann biplane with deflected leading-edge flaps, the baseline Busemann biplane, and the baseline diamond airfoil. Also, Figures 12 and 13 show the pressure coefficient contours around the biplane for different values of free-stream Mach number. It is found from Figure 11 that the leading-edge flaps have the effect of downscaling the wave drag in supersonic flow condition, and also in the range of high-subsonic flow conditions (around 0.7 < M_∞ < 1.0), as compared to the baseline Busemann biplane. Moreover, the drag increase of the biplane due to choked-flow becomes small (as represented by curve B), in contrast to that of the Busemann biplane (represented by curve D). In addition, the change in the area of the front streamline enables a shift of the Mach number, at which the flow is choked in the maximum thickness sections between the two elements, to a lower value M_∞ = 1.41 (in the case of the Busemann biplane, M_∞ = 1.63), which in turns propagates the subsonic area to upstream, forming the bow shock. From Figure 12 (a) to (f), we can observe this process of change of the flow conditions in detail.

As for the area of flow-hysteresis, it is possible to observe that the area is reduced for a range of Mach numbers ($1.41 \leq M_\infty < 1.61$), as compared to that of the Busemann biplane. Then, the flow conditions of flow-hysteresis up to $M_\infty = 1.61$ are represented in Figure 13: As the Mach number increases from $M_\infty = 1.3$, the normal shock wave is formed at the entrance of the biplane, and is swallowed at Mach number $M_\infty = 1.61$, as shown in Figure 13 (f).

These results are consistent with the theoretical values of the start/un-start limits, as indicated before in Figure 6. For the Busemann biplane with deflected leading-edge flaps, the ratio of throat-to-inlet-area is about $A_t/A_i = 0.9$, and therefore, we have found that the leading-edge flaps can be effective in avoiding the choked-flow and flow-hysteresis problems of the Busemann biplane.

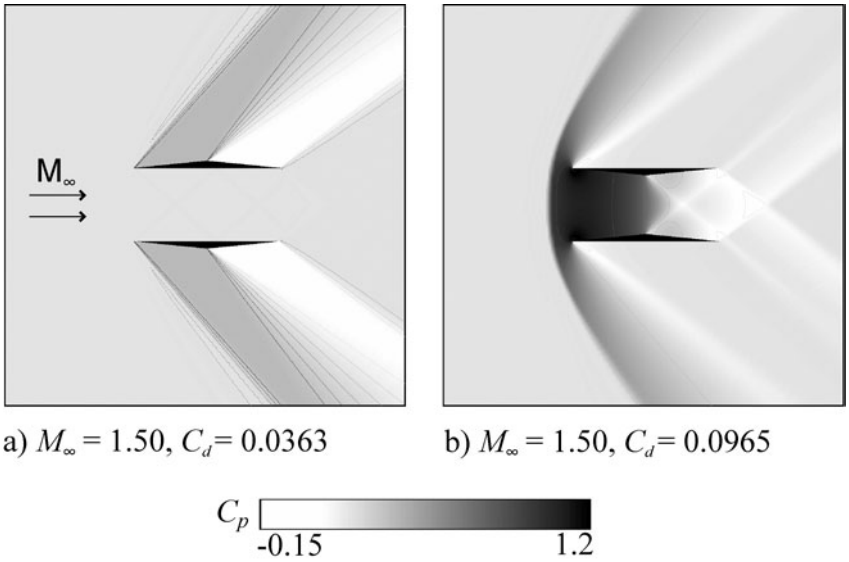

Figure 10. Comparison of the C_p-maps with zero-lift at Mach number $M_\infty = 1.5$: a) diamond airfoil separated into two elements; b) Busemann biplane.

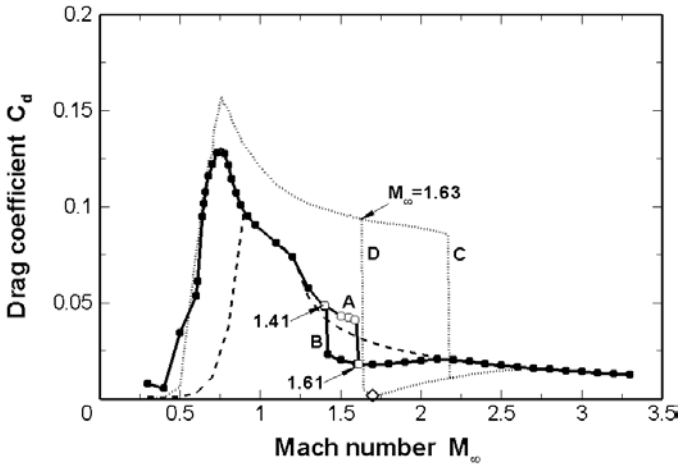

Figure 11. Comparison of the drag characteristics: The solid line represents the Busemann biplane with deflected leading-edge flaps; the dotted line shows the Busemann biplane. In both cases, when accelerating, C_d follows curves A and C. When decelerating, C_d follows curves B and D. Also, the dashed line shows the baseline diamond airfoil. The diamond symbol is the design point at Mach number $M_\infty = 1.7$.

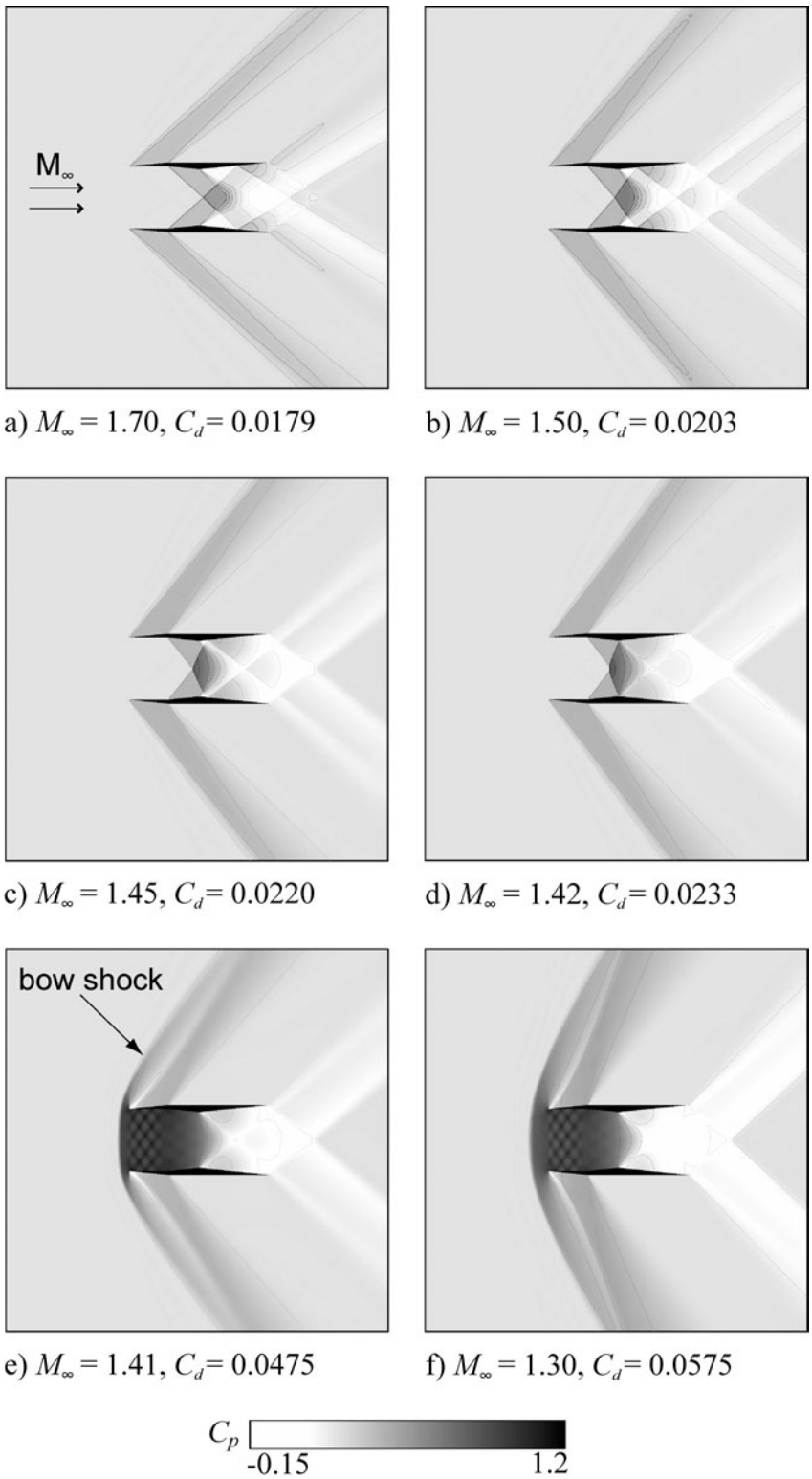

Figure 12. C_p-maps of the Busemann biplane with deflected leading-edge flaps with zero-lift in decelerating condition ($1.3 \leq M_\infty \leq 1.7$).

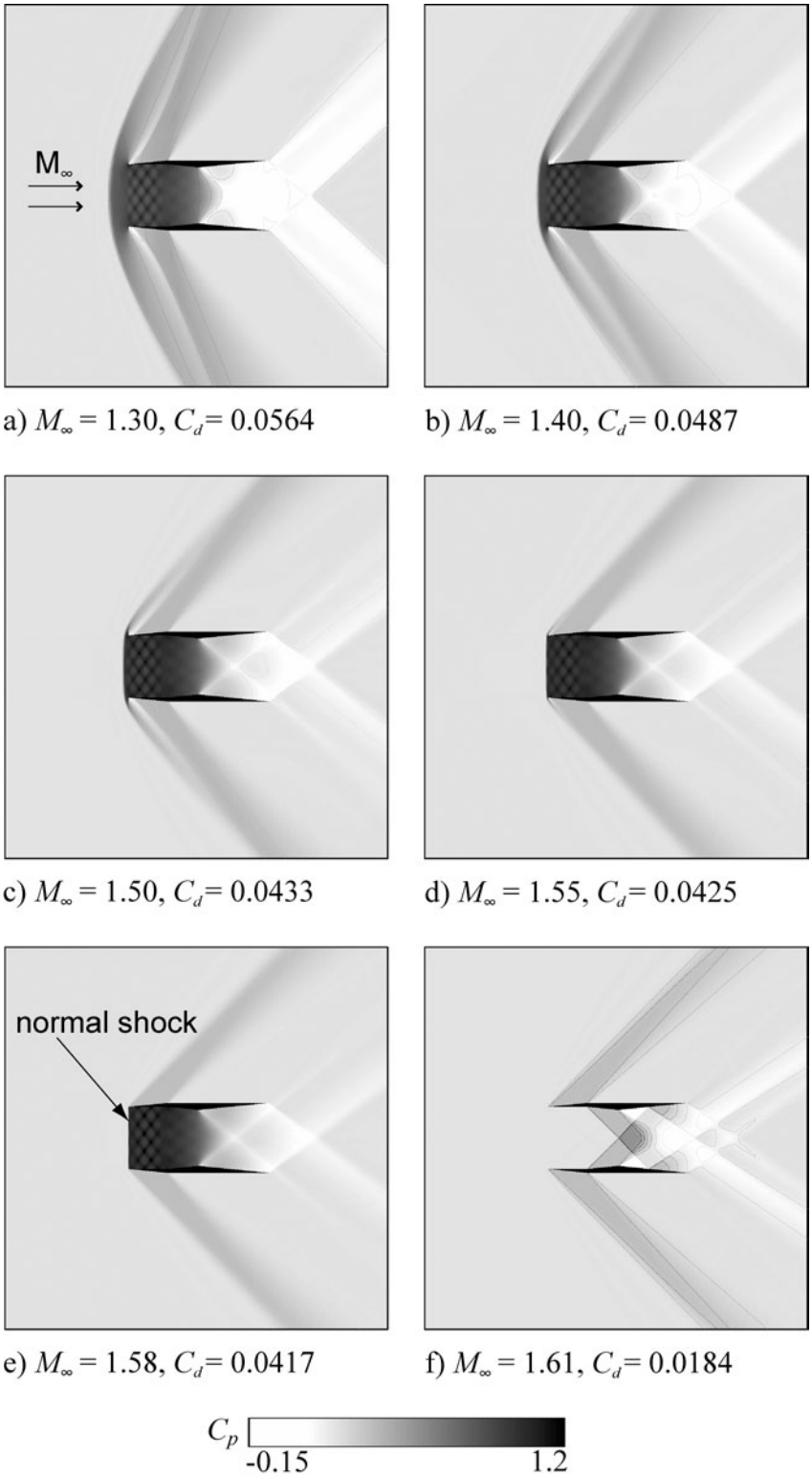

a) $M_\infty = 1.30$, $C_d = 0.0564$ b) $M_\infty = 1.40$, $C_d = 0.0487$

c) $M_\infty = 1.50$, $C_d = 0.0433$ d) $M_\infty = 1.55$, $C_d = 0.0425$

e) $M_\infty = 1.58$, $C_d = 0.0417$ f) $M_\infty = 1.61$, $C_d = 0.0184$

Figure 13. C_p-maps of the Busemann biplane with deflected leading-edge flaps with zero-lift in accelerating condition ($1.3 \leq M_\infty \leq 1.61$).

4.3 Busemann biplane with deflected trailing-edge flaps

In the same way, a comparison of the drag characteristics for the Busemann biplane with deflected trailing-edge flaps, the Busemann biplane, and the baseline diamond airfoil is shown in Figure 14. In addition, the pressure coefficient contours around the biplane are plotted in Figures 15 and 16 for different values of free-stream Mach number. It becomes clear from Figure 14 that the trailing-edge flaps are not effective in avoiding the choked-flow and flow-hysteresis of the Busemann biplane. In fact, the increase in the C_d value due to the choked-flow (curve B) is a little higher with the trailing-edge flaps than in the case of the baseline Busemann biplane (curve D). From the results, we have a C_d value for the biplane equal to $C_d = 0.1040$ at $M_\infty = 1.63$, while the C_d value for the baseline Busemann biplane is $C_d = 0.0944$ at $M_\infty = 1.63$ (both flow conditions are shown in Figure 15 (e) and Figure 4 (e), respectively). Furthermore, the area of flow-hysteresis ($1.63 \leq M_\infty < 2.18$) is exactly the same as compared to that of the Busemann biplane. That is, the bow shock is swallowed at the same Mach number $M_\infty = 2.18$, as shown in Figure 16 (f) and Figure 5 (f).

Here, we would like to focus our attention on the effects of trailing-edge flaps in subsonic flow. Fortunately, we can observe from Figure 14 that the wave drags are decreased between $M_\infty = 0.5$ and $M_\infty = 0.9$, as compared to those of the Busemann biplane. Also, the aerodynamic drag at a speed near to or above the speed of sound is reduced, i.e., the drag-divergence Mach number is shifted to a higher one. Hence, the trailing-edge flaps proved to be actually useful in downscaling the wave drag in subsonic flow conditions.

In order to investigate the reason for the decrease in wave drag at subsonic flow conditions, Figure 17 shows the Mach number distributions of the baseline Busemann biplane and the Busemann biplane with deflected trailing-edge flaps, respectively, where only the supersonic area is represented. In the case of the baseline Busemann biplane, we can confirm that the flow is accelerated between the two airfoil elements. This results in supersonic flow between the two airfoil elements, and also in the generation of the normal shock wave. Thus, as the Mach number increases in subsonic flow, the C_d value is also increased. In the case of the biplane with trailing-edge flaps, on the other hand, the flow between the two elements is moderately accelerated by the trailing-edge flaps, as compared to the Busemann biplane. This results in a slow progression of the formation of a supersonic area between the two elements. Therefore, the wave drags of the biplane with trailing-edge flaps are smaller than those of the baseline Busemann biplane in subsonic flow.

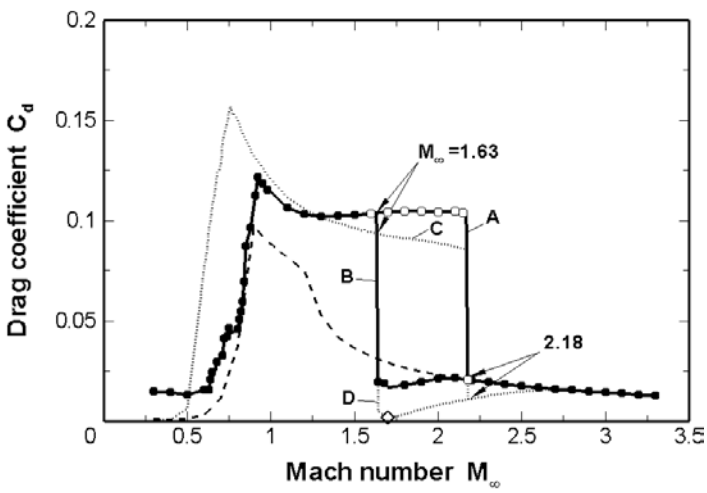

Figure 14. Comparison of the drag characteristics: The solid line represents the Busemann biplane with deflected trailing-edge flaps; the dotted line shows the Busemann biplane. In both cases, when accelerating, C_d follows curves A and C. When decelerating, C_d follows curves B and D. Also, the dashed line shows the baseline diamond airfoil. The diamond symbol is the design point at Mach number $M_\infty = 1.7$.

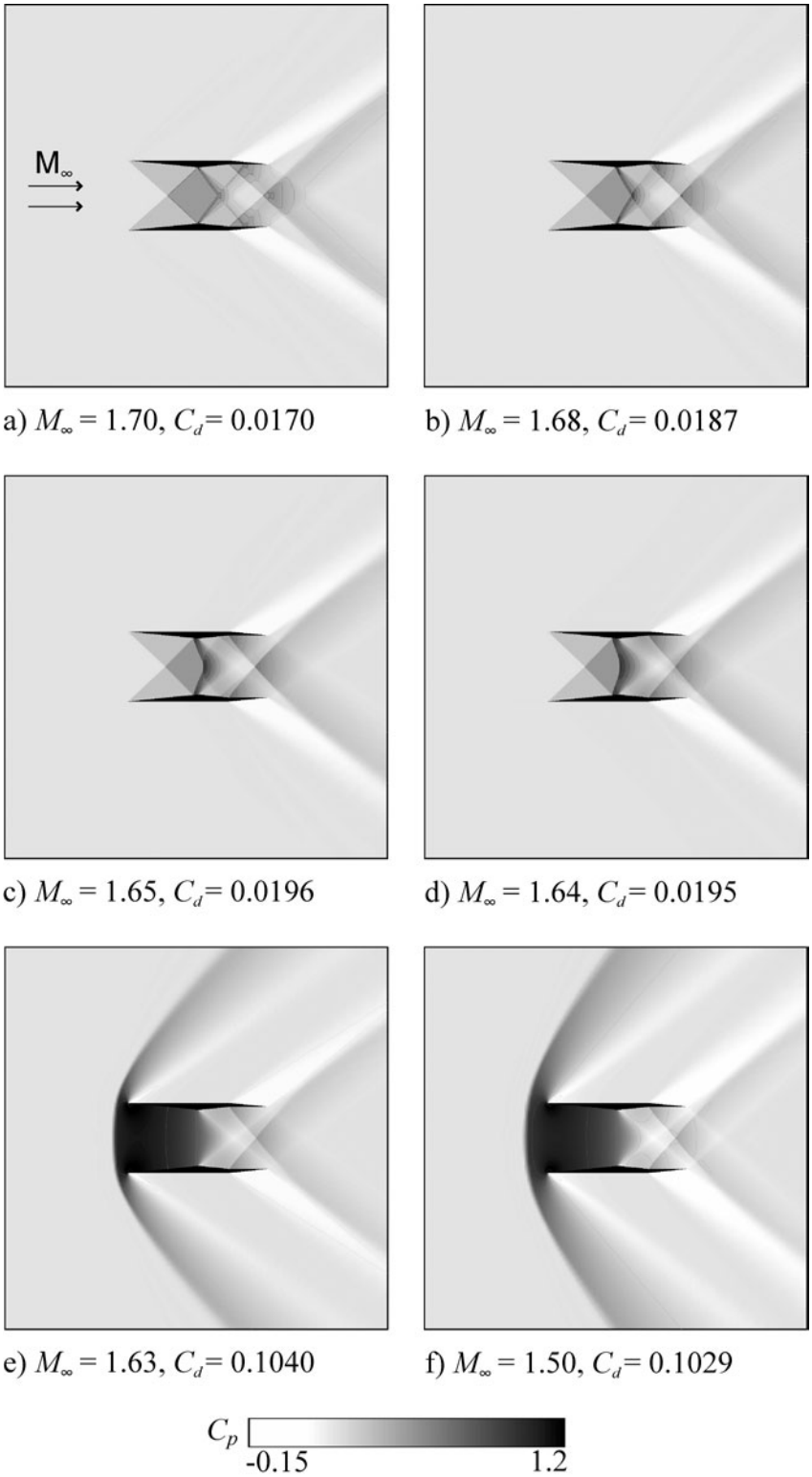

Figure 15. C_p-maps of the Busemann biplane with deflected trailing-edge flaps with zero-lift in decelerating condition ($1.5 \leq M_\infty \leq 1.7$).

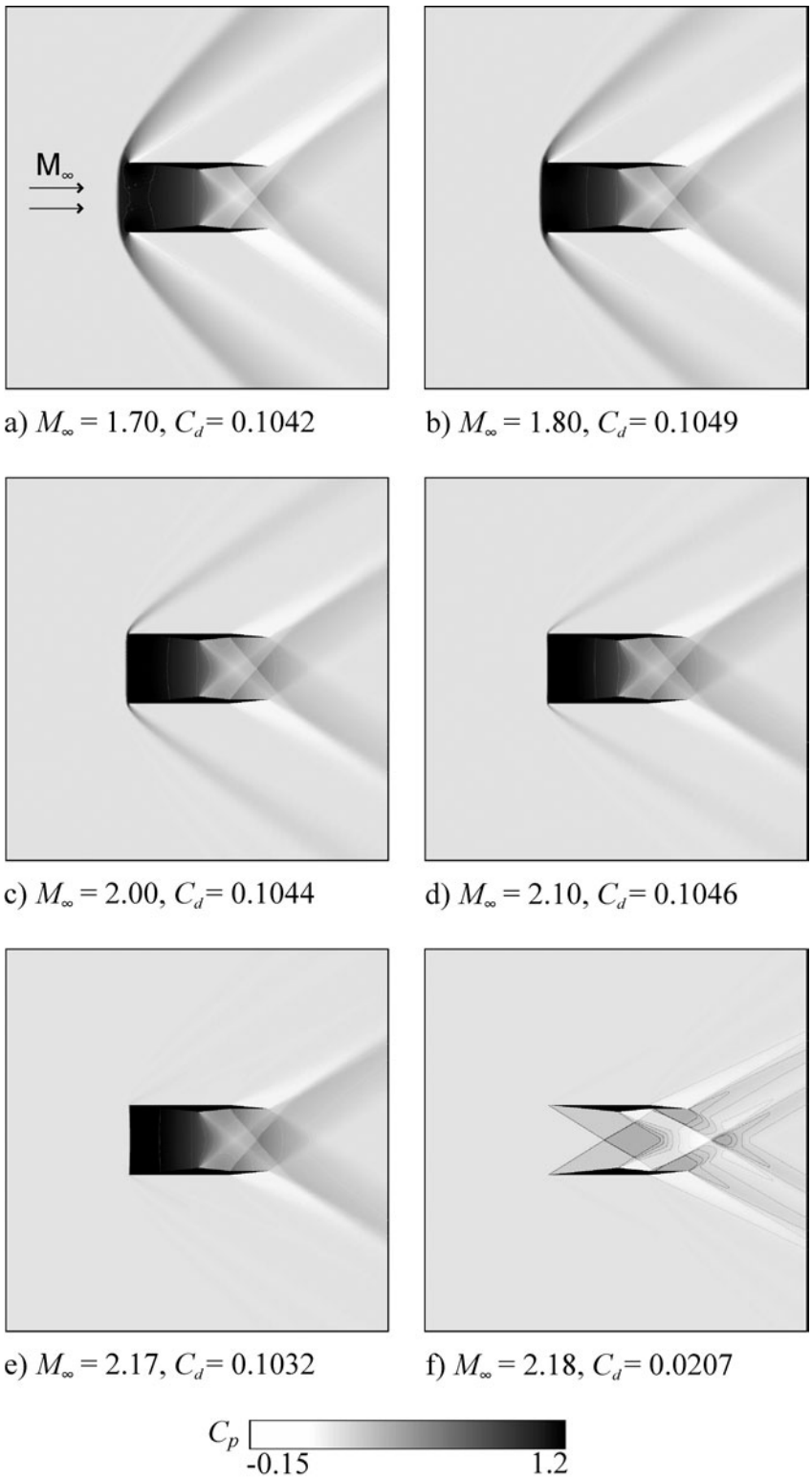

Figure 16. C_p-maps of the Busemann biplane with deflected trailing-edge flaps with zero-lift in accelerating condition ($1.7 \leq M_\infty \leq 2.18$).

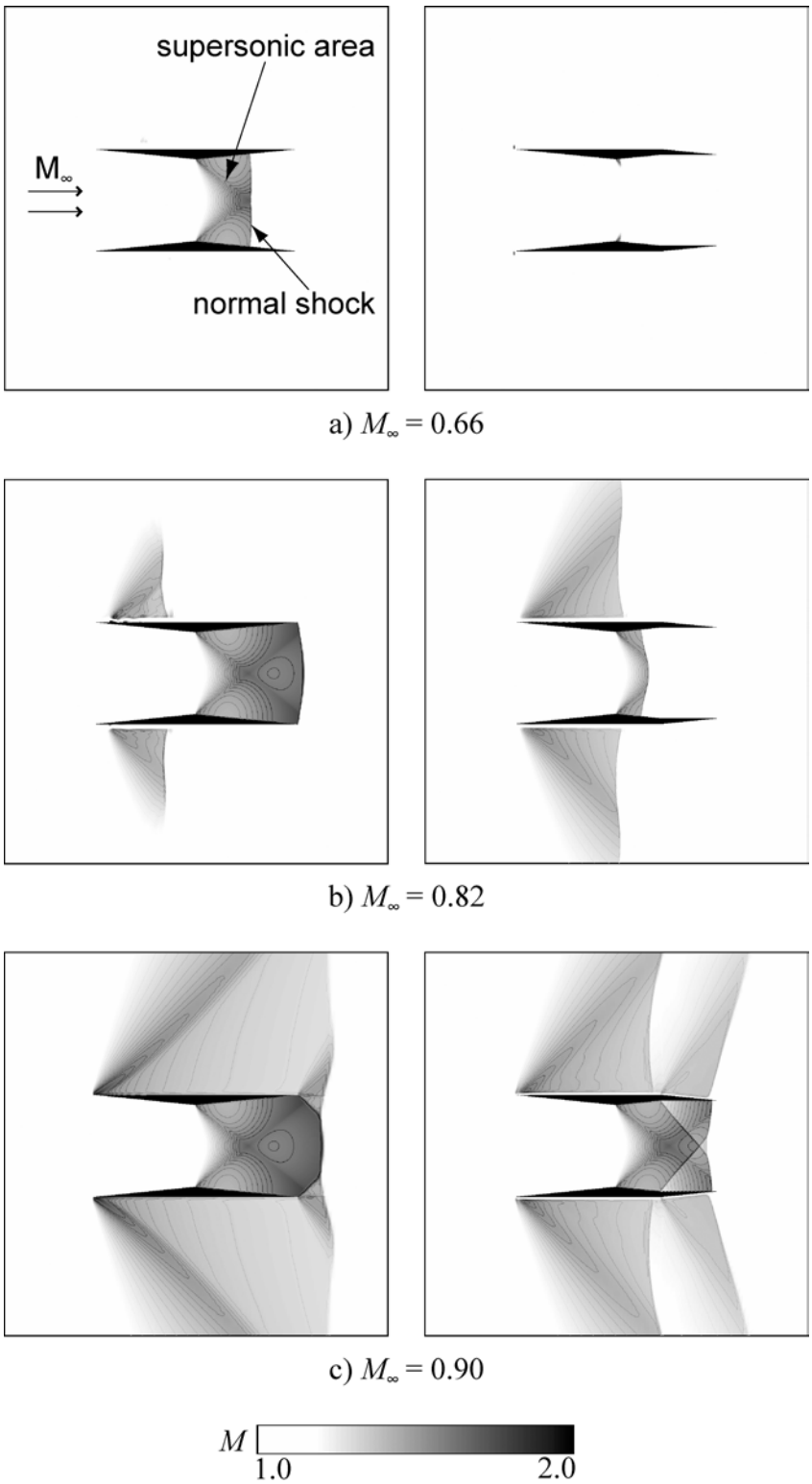

Figure 17. Comparison of the Mach number distributions in subsonic flow conditions: The baseline Busemann biplane is shown in the left row and the Busemann biplane with deflected trailing-edge flaps is shown in the right row. Mach contours in those figures are represented only for supersonic areas. Free-stream Mach numbers are: a) $M_\infty = 0.66$; b) $M_\infty = 0.82$; and c) $M_\infty = 0.9$.

4.4 HLD-1

Finally, Figure 18 plots the drag characteristics of the HLD-1, which includes the previous results for the Busemann biplane and the baseline diamond airfoil. In addition, Figures 19 and 20 show that the pressure coefficient contours around the HLD-1 for different values of free-stream Mach number. From Figure 18, it becomes clear that the wave drag values of the HLD-1 are close to those of the baseline diamond airfoil at all Mach numbers. This result suggests that the HLD-1 utilizes the effects of both the leading and trailing edge flaps in the subsonic and supersonic conditions: In subsonic flow, the HLD-1 can smoothly overcome the sound barrier, as compared to the Busemann biplane, by using the effect of the trailing-edge flaps. In supersonic flow, on the other hand, the increase of C_d due to choked-flow is downscaled (curve B), and also, the flow-hysteresis area is reduced for the range of Mach numbers $1.41 \leq M_\infty < 1.6$ (as the A_t/A_i of HLD-1 is about 0.9), due to the effect of the leading-edge flaps. The processes of choked-flow and flow-hysteresis can be observed in detail in Figures 19 and 20.

Furthermore, we need to pay attention to the fact that the design Mach number is now set at M_∞ = 1.7, in order to use the wave cancellation effect of the Busemann biplane for sonic boom reduction. When the HLD-1 is in accelerating condition (represented by curve A in Figure 18), the bow shock generated in front of the leading-edges is swallowed over at M_∞ = 1.6, as shown in Figure 20 (f). Therefore, if the HLD-1 can be transformed back into the Busemann biplane as the Mach number reaches above M_∞ = 1.64, we can arrive at the design point smoothly from a subsonic regime, i.e., move from the solid line to the dotted line (curve D including the design-point). The reason for this is that once the bow shock has been swallowed over at Mach number M_∞ = 1.64, there is no choked-flow phenomenon at the Busemann biplane, as shown in Figure 4 (a) to (d).

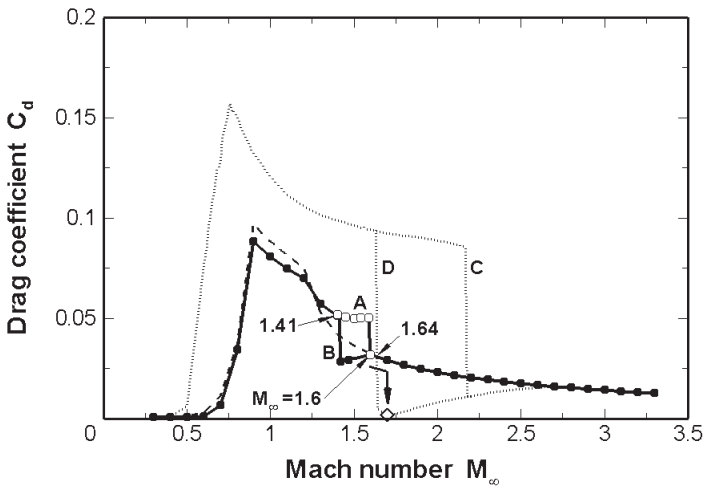

Figure 18. Comparison of the drag characteristics: The solid line represents the HLD-1; the dotted line shows the Busemann biplane. In both cases, when accelerating, C_d follows curves A and C. When decelerating, C_d follows curves B and D. Also, the dashed line shows the baseline diamond airfoil. The diamond symbol is the design point at Mach number M_∞ = 1.7.

5. CONCLUSION

In this paper, four different biplanes have been analyzed, focusing on the use of plain flaps to overcome the problems of choked-flow and flow-hysteresis of the Busemann biplane. From the results, we observed that the leading-edge flaps, by changing the area of the front streamline, can be effective to alleviate the increase in the C_d value due to choked-flow, and also to reduce the area of flow-hysteresis. Also, the flaps could downscale the wave drag in supersonic flow and high-subsonic flow conditions, as compared to the baseline Busemann biplane. On the other hand, the trailing-edge flaps were not effective in avoiding the choked-flow and flow-hysteresis. However, these flaps were useful in downscaling the wave drag in subsonic flow conditions, which resulted in a smooth transition from subsonic to supersonic flow as compared to the baseline Busemann biplane. In addition, it was found that the biplane equipped with both flaps could benefit from both effects; arriving at the design point smoothly from subsonic conditions, and avoiding the severe drag penalty due to choked-flow and flow-

hysteresis. As a conclusion, we would like to note that the use of flaps is a highly plausible solution to the problems of choked-flow and flow-hysteresis of the Busemann biplane under off-design conditions, since it will not only overcome these problems, but it also has applications as a high-lift device for takeoff and landing conditions.

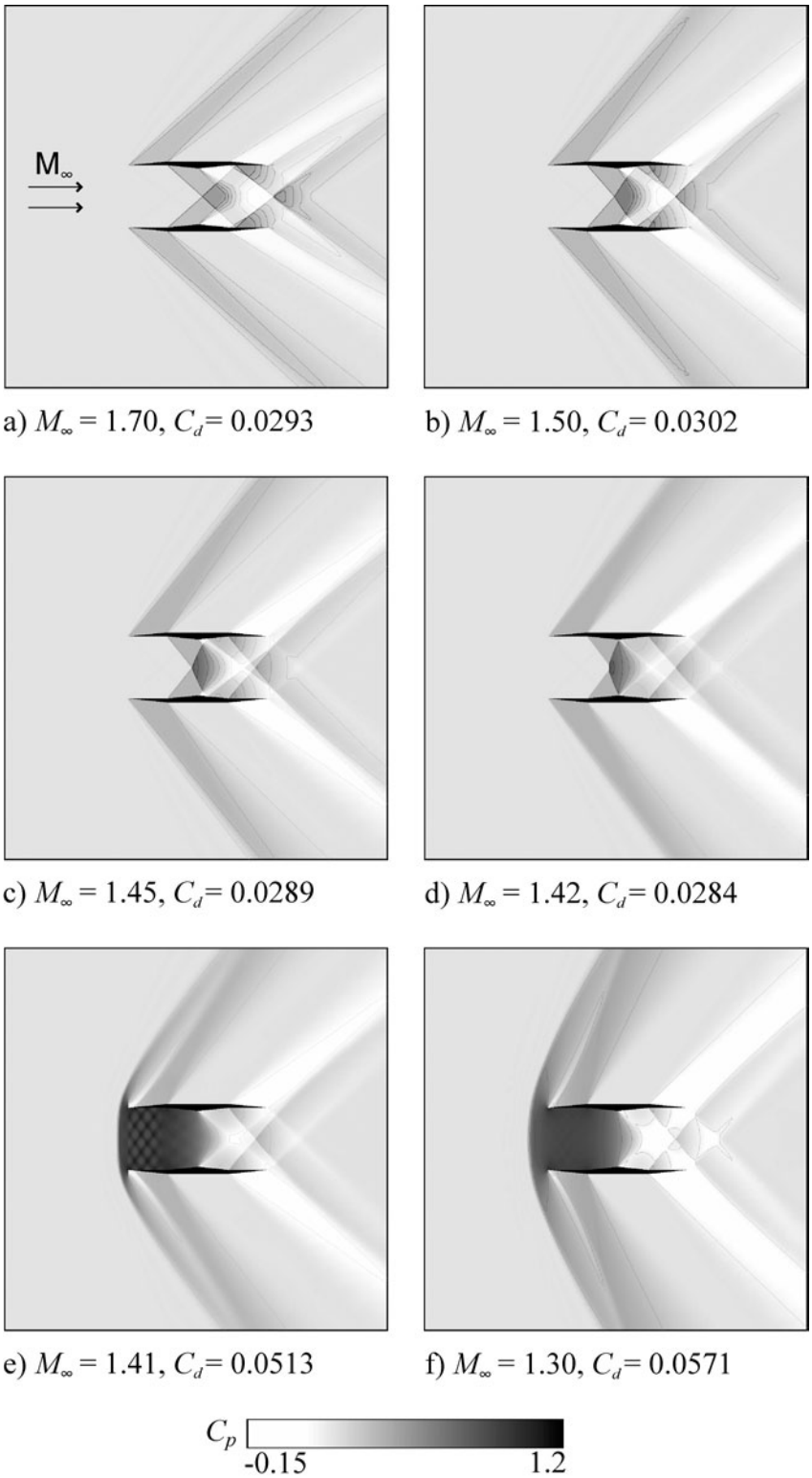

Figure 19. C_p-maps of the HLD-1 with zero-lift in decelerating condition ($1.3 \leq M_\infty \leq 1.7$).

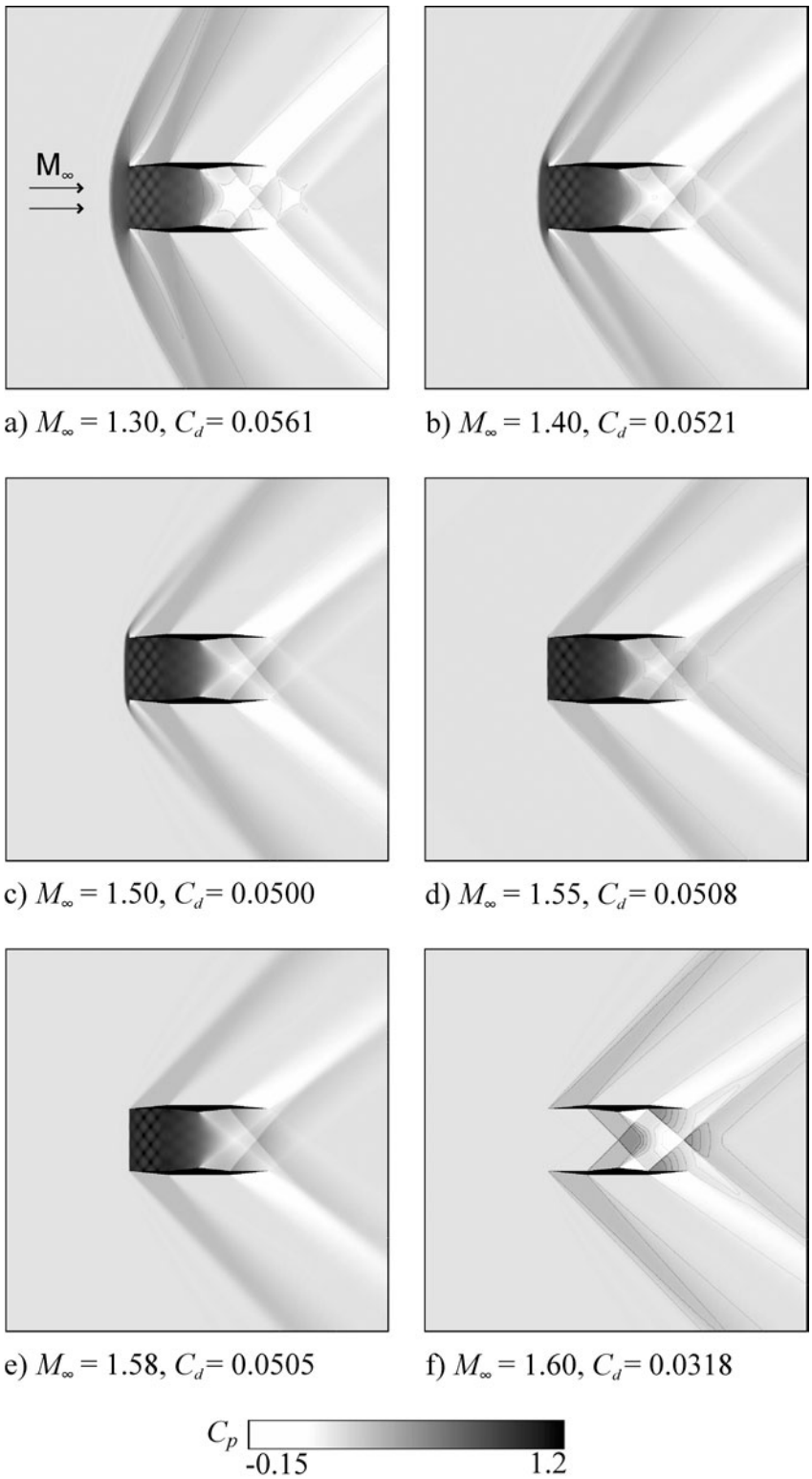

Figure 20. C_p-maps of the HLD-1 with zero-lift in accelerating condition ($1.3 \leq M_\infty \leq 1.6$).

APPENDICES

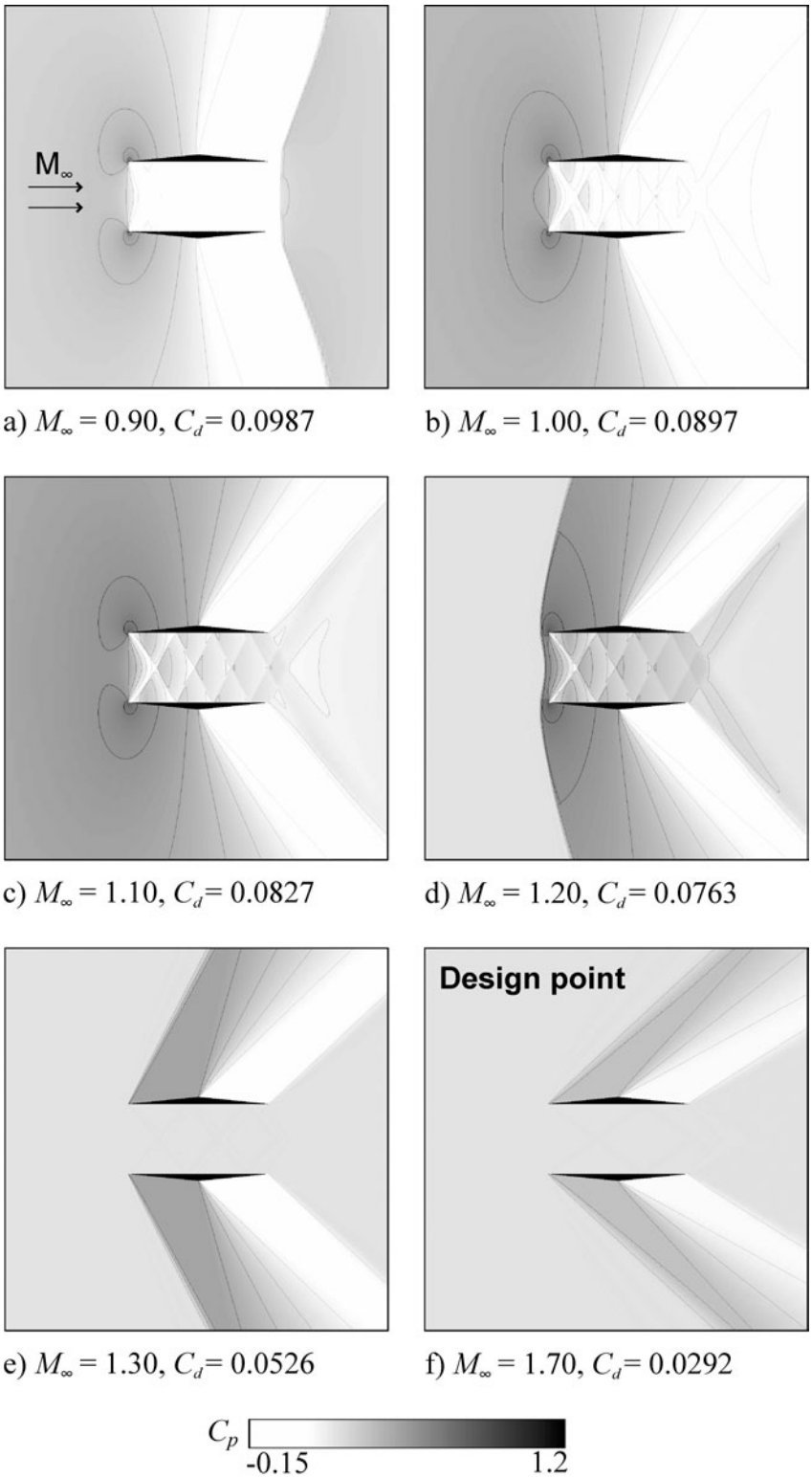

a) $M_\infty = 0.90$, $C_d = 0.0987$ b) $M_\infty = 1.00$, $C_d = 0.0897$

c) $M_\infty = 1.10$, $C_d = 0.0827$ d) $M_\infty = 1.20$, $C_d = 0.0763$

e) $M_\infty = 1.30$, $C_d = 0.0526$ f) $M_\infty = 1.70$, $C_d = 0.0292$

Appendix A: C_p-maps of the diamond airfoil separated into two elements with zero-lift condition (α = 0 deg., $0.9 \leq M_\infty \leq 1.7$).

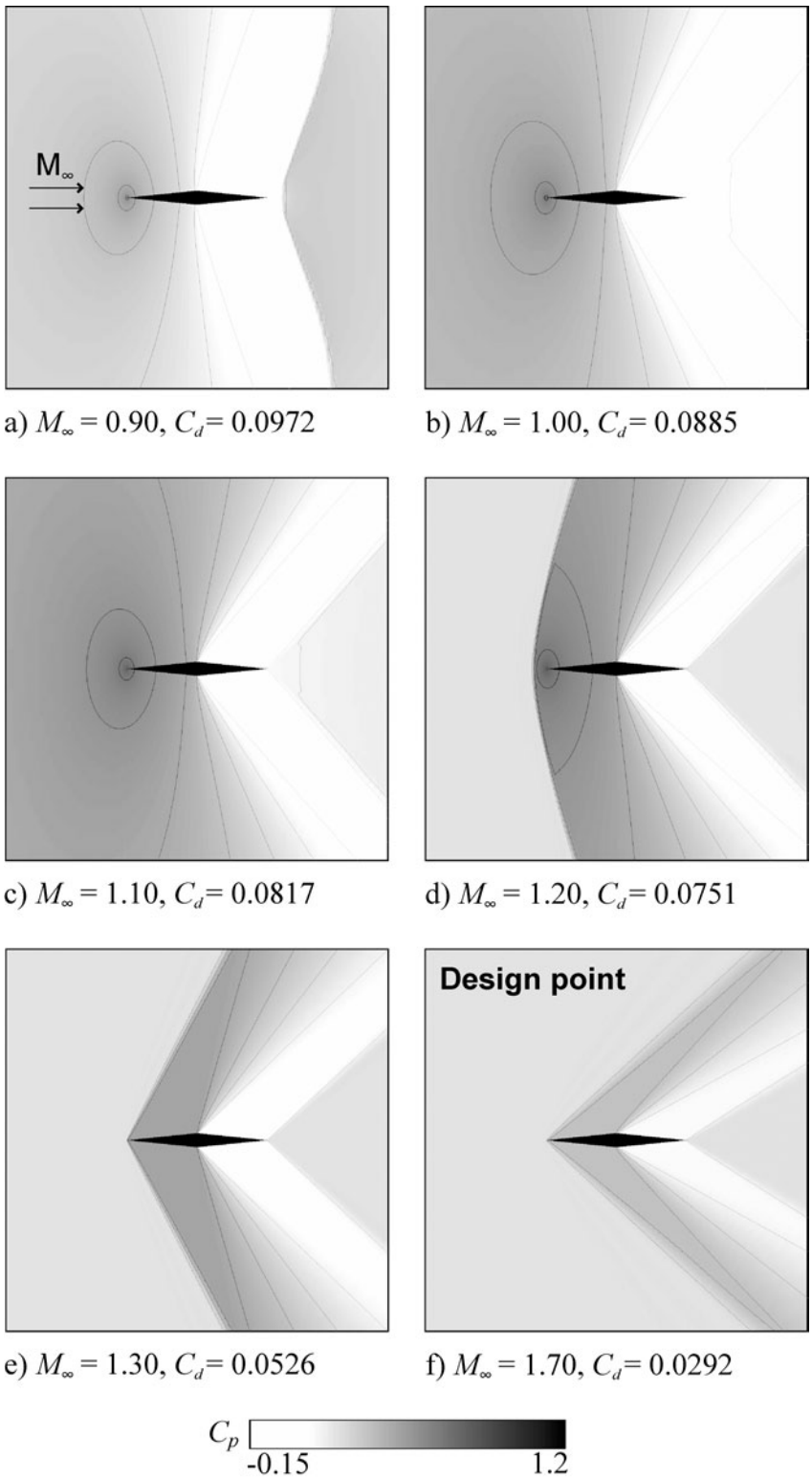

a) $M_\infty = 0.90$, $C_d = 0.0972$ b) $M_\infty = 1.00$, $C_d = 0.0885$

c) $M_\infty = 1.10$, $C_d = 0.0817$ d) $M_\infty = 1.20$, $C_d = 0.0751$

e) $M_\infty = 1.30$, $C_d = 0.0526$ f) $M_\infty = 1.70$, $C_d = 0.0292$

Appendix B: C_p-maps of the baseline diamond airfoil with zero-lift condition ($\alpha = 0$ deg., $0.9 \leq M_\infty \leq 1.7$).

ACKNOWLEDGMENTS

The author wishes to thank Associate Prof. K. Matsushima of Tohoku University and Associate Prof. M. Kanazaki of Tokyo Metropolitan University for their invaluable teachings and comments for this research. The author also wishes to gratefully acknowledge my colleagues, especially Ms. J. N. Lim and Mr. F. K. Nakabayashi, in publishing this paper. This research was supported by a grant from the Research Fellowships of the Japan Society for the Promotion of Science for young Scientists.

REFERENCES

1. Trubshaw, B., *Concorde: the Inside Story*, Sutton Publishing Limited, Phoenix Mill, Thrupp, Stroud, Gloucestershire, 2000.
2. Chudoba, B., Coleman, G., Oza, A. and Czysz, P. A., What Price Supersonic Speed? A Design Anatomy of Supersonic Transportation Part1, *The Aeronautical Journal*, 2008, 112(1129), 141-151.
3. Chudoba, B., Oza, A., Coleman, G. and Czysz, P. A., What Price Supersonic Speed? An Applied Market Research Case Study Part2, *The Aeronautical Journal*, 2008, 112(1130), 219-231.
4. Robert, J. M., A Supersonic Business-Jet Concept Designed for Low Sonic Boom, *NASA TM-2003-212435*, 2003.
5. Yoshida, K. and Makino, Y., Aerodynamic Design of Unmanned and Scaled Supersonic Experimental Airplane in Japan, *Proceedings of the ECCOMAS 2004*, Finland, 2004.
6. Makino, Y. and Kroo, I., Robust Objective Functions for Sonic-Boom Minimization, *Journal of Aircraft*, 2006, 43(5), 1301-1306.
7. Makino, Y., Aoyama, T., Iwamiya, T., Watanuki, T. and Kubota, H., Numerical Optimization of Fuselage Geometry to Modify Sonic-Boom Signature, *Journal of Aircraft*, 1999, 36(4), 668-674.
8. FAR 91.817, Part 91, General Operating and Flight Rules Subpart I – Operating Noise Limits, Federal Airworthiness Administration, Department of Transportation.
9. Pawlowski, J. W., Graham, D. H., Boccadoro, C, H., Coen, P. G. and Maglieri, D. J., Origins and Overview of the Shaped Sonic Boom Demonstration Program, *AIAA Paper*, AIAA-2005-0005, 2005.
10. Plotkin, K. J., Haering, E. A. Jr., Murray, J. E., Maglieri, D. J., Salamone, J., Sullivan, B. M. and Schein, D., Ground Data Collection of Shaped Sonic Boom Experiment Aircraft Pressure Signatures, *AIAA Paper*, AIAA-2005-0010, 2005.
11. Plotkin, K. J., Martin, R., Maglieri, D. J., Haering, E. A. Jr. and Murray, J. E., Pushover Focus Booms from the Shaped Sonic Boom Demonstrator, *AIAA Paper*, AIAA-2005-0011, 2005.
12. Morgenstern, J. M., Arslan, A., Lyman V. and Vadyak, J., F-5 Shaped Sonic Boom Demonstrator's Persistence of Boom Shaping Reduction through Turbulence, *AIAA Paper*, AIAA-2005-0012, 2005.
13. Henne, P. A., Case for Small Supersonic Civil Aircraft, *Journal of Aircraft*, 2005, 42(3), 765-774.
14. Howe, D. C., Improved Sonic Boom Minimization with Extendable Nose Spike, *AIAA Paper*, AIAA-2005-1014, 2005.
15. Cowart, R. and Grindle, T., An Overview of the Gulfstream / NASA Quiet Spike™ Flight Test Program, *AIAA Paper*, AIAA-2008-0123, 2008.
16. Howe, D. C., Simmons, III, F. and Freund, D., Development of the Gulfstream Quiet Spike™ for Sonic Boom Minimization, *AIAA Paper*, AIAA-2008-0124, 2008.
17. Howe, D. C., Waithe, K. A. and Haering, E. A. Jr., Quiet Spike™ Near Field Flight Test Pressure Measurements with Computational Fluid Dynamics Comparisons, *AIAA Paper*, AIAA-2008-0128, 2008.
18. Smith, H., A Review of Supersonic Business Jet Design Issues, *The Aeronautical Journal*, 2007, 111(1126), 761-776.
19. Kusunose, K., A New Concept in the Development of Boomless Supersonic Transport, *Proceedings of the First International Conference on Flow Dynamics*, Sendai, Japan, 2004, 46-47.
20. Kusunose, K., Matsushima, K., Goto, Y., Yamashita, H., Yonezawa, M., Maruyama, D. and Nakano, T., A Fundamental Study for the Development of Boomless Supersonic Transport Aircraft, *AIAA Paper*, AIAA-2006-0654, 2006.

21. Liepmann, H. W. and Roshko, A., *Elements of Gas Dynamics*, John Wiley & Sons, Inc., New York, 1957, 107-123, 389.
22. Matsushima, K., Kusunose, K., Maruyama, D. and Matsuzawa, T., Numerical Design and Assessment of a Biplane as Future Supersonic Transport – Revisiting Busemann's Biplane, *Proceedings of the 25th ICAS Congress*, ICAS 2006-3.7.1, 1-10, Hamburg, Germany, 2006.
23. Maruyama, D., Matsushima, K., Kusunose, K. and Nakahashi, K., Aerodynamic Design of Biplane Airfoils for Low Wave Drag Supersonic Flight, *AIAA Paper*, AIAA-2006-3323, 2006.
24. Maruyama, D., Matsushima, K., Kusunose, K. and Nakahashi, K., Aerodynamic Design of Three-dimensional Low Wave-drag Biplanes Using Inverse Problem Method, *AIAA Paper*, AIAA-2008-0289, 2008.
25. Kusunose, K., Matsushima, K., Obayashi, S., Furukawa, T., Kuratani, N., Goto, Y., Maruyama, D., Yamashita, H. and Yonezawa, M., *Aerodynamic Design of Supersonic Biplane: Cutting Edge and Related Topics*, The 21st Century COE Program, International COE of Flow Dynamics Lecture Series, Vol. 5, Tohoku University Press, Sendai, Japan, 2007.
26. Yonezawa, M., Yamashita, H., Obayashi, S. and Kusunose, K., Investigation of Supersonic Wing Shape Using Busemann Biplane Airfoil, *AIAA Paper*, AIAA-2007-0686, 2007.
27. Kuratani, N., Ogawa, T., Yamashita, H., Yonezawa, M. and Obayashi, S., Experimental and Computational Fluid Dynamics around Supersonic Biplane for Sonic-Boom Reduction, *AIAA Paper*, AIAA-2007-3674, 2007.
28. Yamashita, H., Yonezawa, M., Obayashi, S. and Kusunose, K., A Study of Busemann-type Biplane for Avoiding Choked Flow, *AIAA Paper*, AIAA-2007-0688, 2007.
29. Aksel, M. H. and Eralp, O. C., *Gas Dynamics*, Prentice Hall Inc., Englewood Cliffs, 1994, Chap. 5, 186-195.
30. Van Wie, D. M., Kwok, F. T. and Walsh, R. F., Starting Characteristics of Supersonic Inlets, *AIAA Paper*, AIAA-1996-2914, 1996.
31. Takaki, R., Yamamoto, K., Yamane, T., Enomoto, S. and Mukai, J., The Development of the UPACS CFD Environment, *Proceedings of the 5th International Symposium, ISHPC 2003*, Springer, Tokyo, 2003, 307-319.